

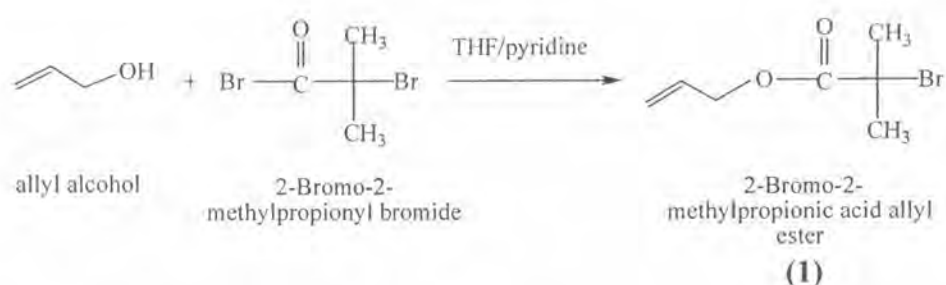
CHAPTER IV

RESULTS AND DISCUSSION

In this chapter, the results are divided into four sections. The first section mainly focuses on the synthesis of surface-tethered poly(*tert*-butyl acrylate) (*Pt*-BA) brushes from silicon-supported α -bromoisobutyrate monolayer by surface-initiated atom transfer radical polymerization (ATRP) of *tert*-butyl acrylate (*t*-BA). The second section explains the synthesis of surface-tethered poly(acrylic acid) (PAA) brushes by hydrolysis of the surface-tethered *Pt*-BA brushes to remove *tert*-butyl groups. The third section involves the fabrication of multilayer film on the surface-tethered PAA brushes. The final section addresses bioactivity tests of the multilayer film deposited on the surface-tethered PAA brushes.

4.1 Synthesis of α -Bromoester to be used as Initiators

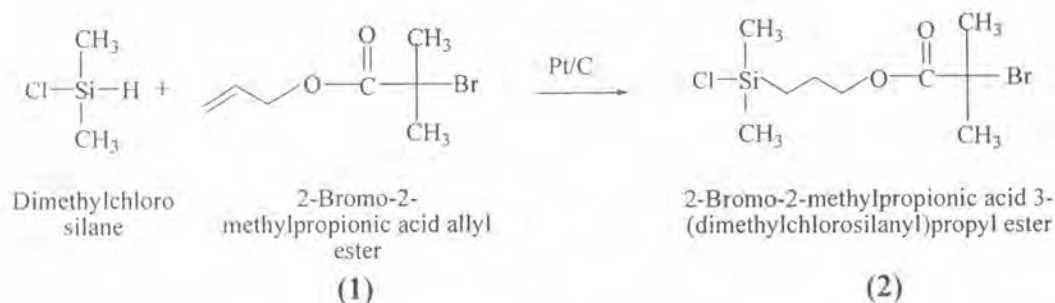
4.1.1 Synthesis of 2-Bromo-2-methylpropionic acid allyl ester (**1**)



The esterification of allyl alcohols with 2-bromo-2-methylpropionyl bromide in tetrahydrofuran gave 2-bromo-2-methylpropionic acid allyl ester (**1**) as colorless liquid product which was sufficiently pure for the next synthesis without further purification after the work-up process. The ¹H NMR (Figure A-1) of the product (**1**) shows the doublet of doublet signal and a multiplet signal of alkene protons; (CH₂=CH) at 5.25-5.40 ppm and (CH₂=CH) at 5.88-5.98 ppm, respectively. The doublet signal of methylene protons (OCH₂) at 4.71 ppm and a singlet signals of the

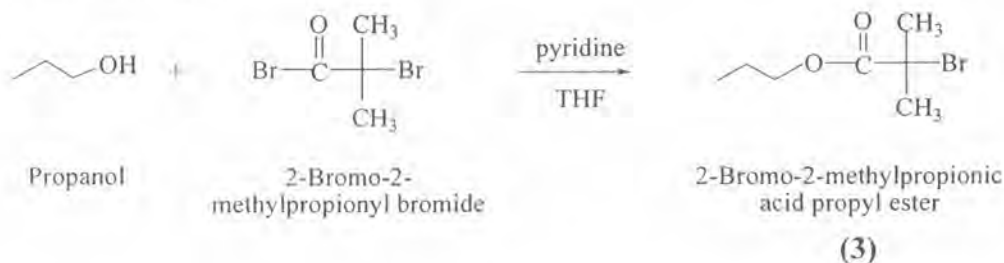
methyl protons of $C(CH_3)_2$ at 1.98 ppm indicate the complete reaction between allyl alcohol and 2-bromo-2-methylpropionyl bromide.

4.1.2 Synthesis of 2-Bromo-2-methylpropionic acid 3-(dimethylchlorosilanyl)propyl ester (2)



Hydrosilation of dimethylchlorosilane with (1) was carried out by refluxing in the presence of Pt/C catalyst for 15 h. The crude product of 2-bromo-2-methylpropionic acid 3-(dimethylchlorosilanyl)propyl ester (2) was a light-yellow oil. The $^1\text{H-NMR}$ spectrum (Figure A.2) of the product (2) shows a triplet signal and a multiplet signal of the methylene protons of $(\text{SiCH}_2\text{CH}_2\text{CH}_2\text{O})$ and $(\text{SiCH}_2\text{CH}_2\text{CH}_2\text{O})$ at 0.58 and 1.65-1.80 ppm, respectively. The multiplet peak of protons $(\text{CH}_2=\text{CH})$ at 5.25-5.40 ppm and $(\text{CH}_2=\text{CH})$ at 5.88-5.98 ppm from the starting alkene (1) disappeared after the reaction indicating the completion of reaction.

4.1.3 Synthesis of 2-Bromo-2-methylpropionic acid propyl ester (3) as a "Sacrificial" Initiator



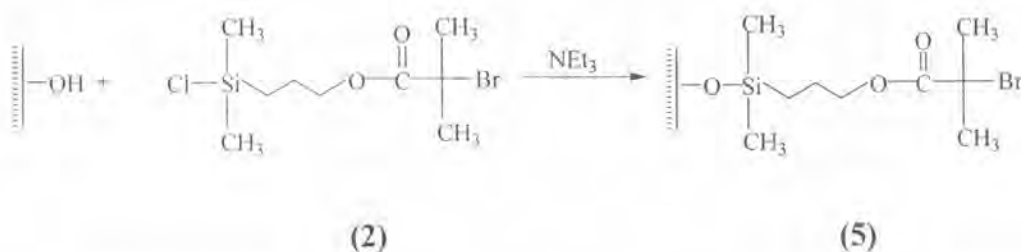
The esterification of 1-propanol with 2-bromo-2-methylpropionyl bromide in tetrahydrofuran gave 2-bromo-2-methylpropionic acid propyl ester (3) as a light-yellow viscous liquid. The $^1\text{H-NMR}$ (Figure A-3) of the product (3) showed a singlet signal of

the methyl protons $C(\text{CH}_3)_2$ at 1.96 ppm and a triplet signal of the methylene protons (OCH_2) at 4.14 ppm indicating the success of the reaction between 1-propanol and 2-bromo-2-methylpropionyl bromide. This product was used as an “added” or “sacrificial” initiator for the polymerization of polymer brushes.

4.2 Preparation of Poly(*tert*-Butyl Acrylate) Brushes

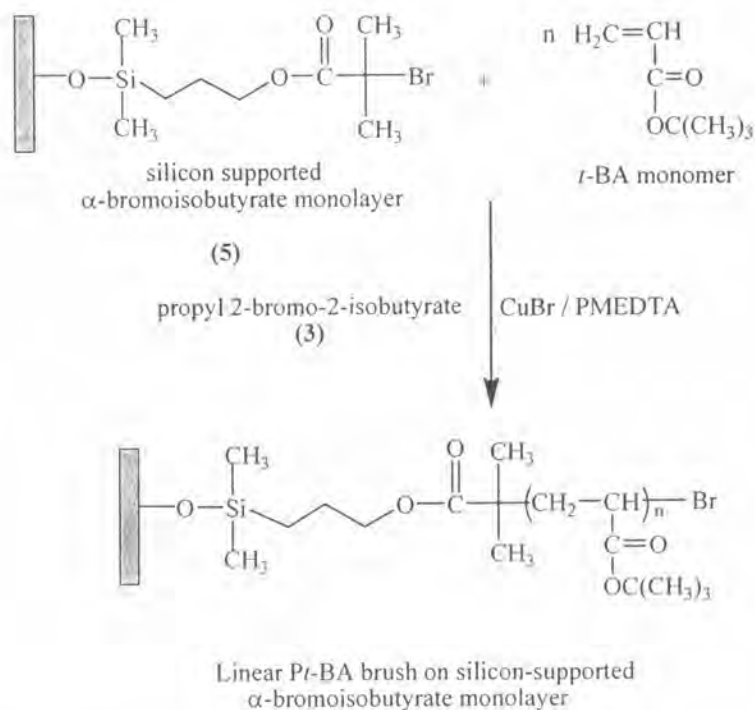
This section mainly focuses on the synthesis of *Pt*-BA brushes. *Pt*-BA brushes were grown from the surface grafted α -bromoisobutyrate monolayer *via* ATRP at 62°C in the presence of CuBr/PMEDTA using acetone as a solvent.

4.2.1 Preparation of Surface Grafted α -Bromoester Initiators (5)



Advancing/receding water contact angle of silicon-supported α -bromoisobutyrate monolayer was 69°/58° which was significantly different from the value of 28°/17° for the cleaned and dried hydrophilic silicon substrates. This result indicates that the α -bromoisobutyrate monolayer was formed.

4.2.2 Surface-initiated Polymerization of *tert*-Butyl Acrylate



1) Confirmation of *Pt*-BA Brushes Formation

The FT-IR spectra of silica particles grafted with α -bromoisobutyrate monolayer and *Pt*-BA brushes are depicted in comparison with the unmodified silica particles in Figure 4.1. There is a shoulder peak appearing at 1727 cm^{-1} in Figure 4.1b due to the carbonyl stretching of ester from α -bromoisobutyrate monolayer on the silicon surface before the formation of polymer brushes. The spectra in Figure 4.1b shows the C-H stretching at 2935 and 2978 cm^{-1} , CH_3 bending at 1369 cm^{-1} , and C=O stretching at 1727 cm^{-1} indicating the success of *Pt*-BA formation.

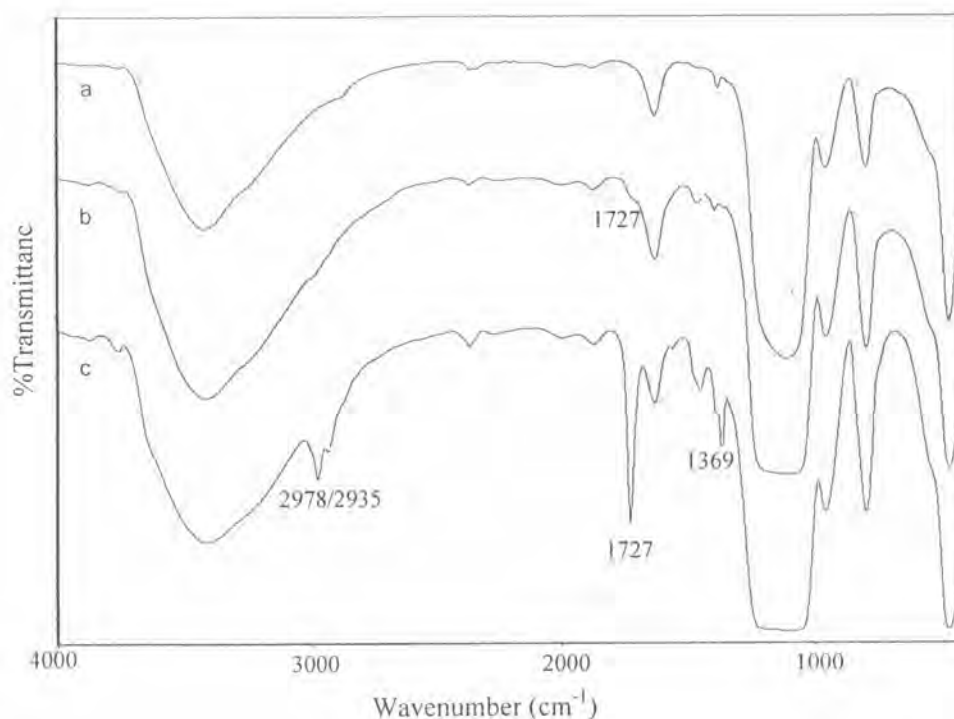
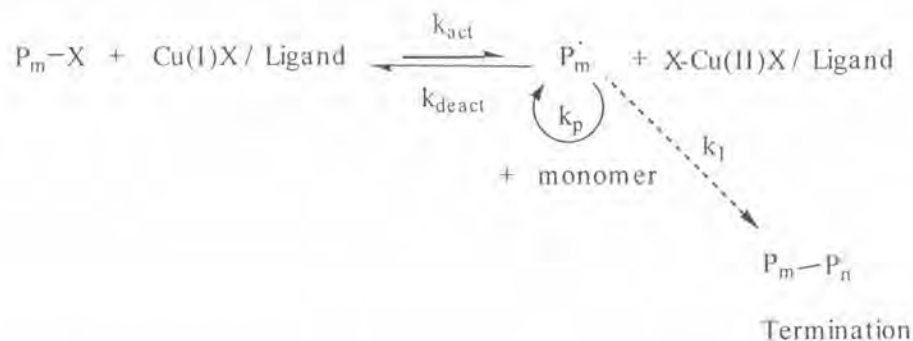


Figure 4.1 FT-IR spectra of silica particles (a), silica particles with surface-tethered α -bromoisobutyrate monolayer (b) and Pt-BA brushes having $\overline{M}_n = 20760$ on silica particles (c)

2) Molecular Weight and Graft Density of Pt-BA Brushes

It is rather difficult to obtain the molecular weight of the polymer brush directly since the amount of polymer on the silicon substrate is too small to degraft and analyze. The polymer formed by the free initiator (“sacrificial” initiator) in the solution was then used to monitor the surface-initiated polymerization process and molecular weight. It has been proven that the molecular weight and polydispersity of the graft polymer were nearly equal to those of the free polymer produced in the solution, meaning that the free polymer is a good measure of the characteristics of the graft polymer. [83] The free initiator plays a role not only as an indicator of the polymerization but also as a controller for the ATRP on the surface. The concentration of the Cu^{II} complex produced from the reaction at the substrate surface is too low to reversibly deactivate polymer radicals with a sufficiently high rate. The addition of the free initiator creates the necessary concentration of the $\text{Cu}(\text{II})$

complex, which in turn controls polymerization from the substrate as well as in solution (Scheme 4.1).



Scheme 4.1 The activation/deactivation cycles of ATRP process

Figure 4.2 shows the change in the molecular weight (\overline{M}_n) and molecular weight distribution ($\overline{M}_w/\overline{M}_n$) of the free Pt-BA as a function of polymerization time at two targeted degrees of polymerization (DP): DP = 100 and 200. The monomer concentration ($[t\text{-BA}]$) of 4.6 M and the molar ratio of $[I]/[\text{CuBr}]/[\text{PMDETA}]$ of 1:1:1 were fixed in these experiments. The amount of free initiator was varied to obtain the targeted DP. The molecular weight increased with an increase of the targeted DP. For both targeted DPs, the molecular weight increased linearly with increasing polymerization time. The highest molecular weight obtained was in accord with the targeted DP. The molecular weight distribution being close to 1.0 suggested that the polymerization mechanism is living.

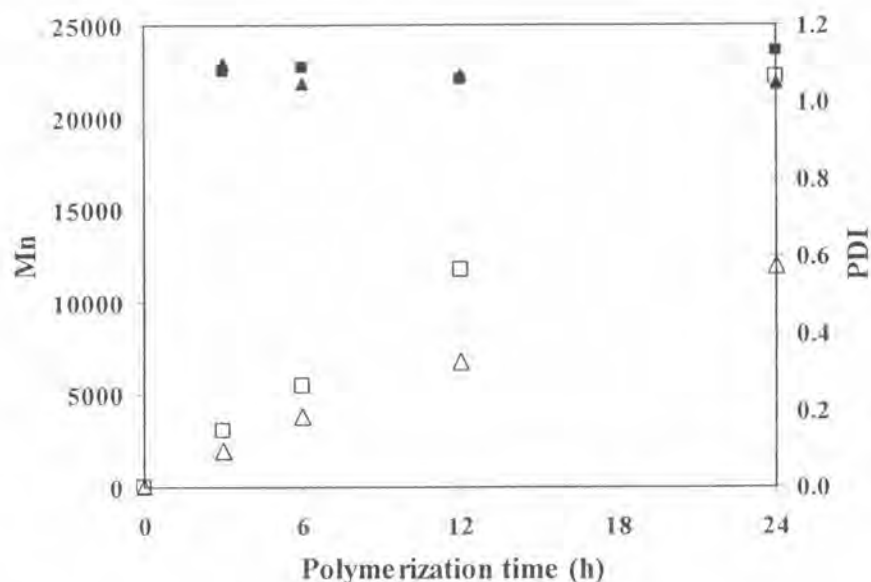


Figure 4.2 Molecular weight (\overline{M}_n): targeted DP = 100 (Δ) and 200 (\square) and molecular weight distribution ($\overline{M}_w/\overline{M}_n$): targeted DP = 100 (\blacktriangle) and 200 (\blacksquare) of Pt-BA as a function of polymerization time

The information related to molecular weight and thickness can be used to calculate a grafting density of polymer brushes. The grafting density (σ) which is a unit per cross-sectional area (A_x) per chain can be determined from the corresponding film thickness (t) and the molecular weight of the chain (M_n) from the following equation:

$$\sigma = \frac{1}{A_x} = \frac{t\rho N_A}{M_n} \quad (4.1)$$

Where ρ is the mass density (1.03 g/cm³ for Pt-BA) and N_A is Avogadro's number. Using slopes obtained from the plots in Figure 4.3 which correspond to t/M_n , the calculated grafting density is 0.37 and 0.34 chains/nm² and unit per cross-sectional area is 2.70 and 2.94 nm²/chain for the targeted DP = 100 and 200, respectively. These results agree quite well with the data previously reported that the grafting densities for various polymers prepared by surface-initiated ATRP were also ranged from 0.1 to 0.6 chains/nm² [84].

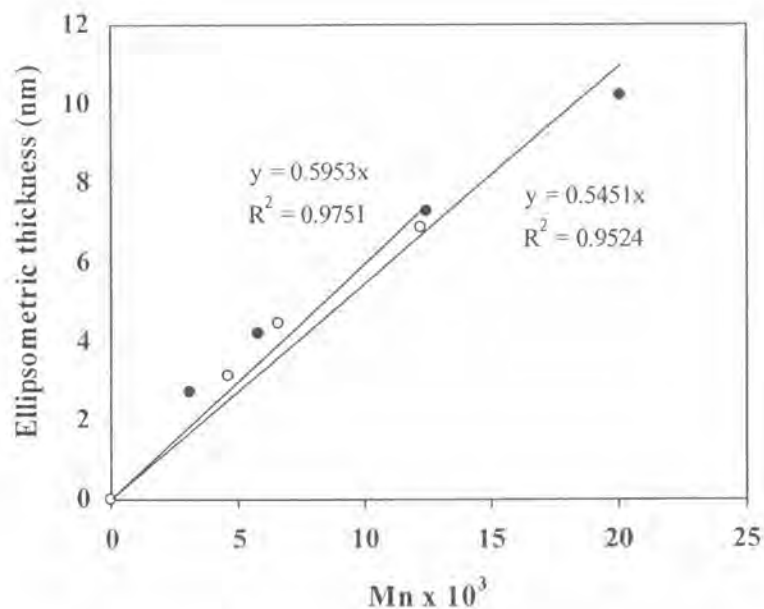


Figure 4.3 Relationship between the ellipsometric thickness of *Pt*-BA brushes with molecular weight of free *Pt*-BA for targeted DP = 100 (○) and 200 (●).

The growth of *Pt*-BA brushes can also be monitored by water contact angle analysis. Figure 4.4 illustrates advancing (θ_A) and receding (θ_R) water contact angles of silicon-supported *Pt*-BA brushes as a function of polymerization time. Both advancing (θ_A) and receding (θ_R) contact angles rapidly increased from $69^\circ/58^\circ$ for the silicon-supported α -bromoisobutyrate monolayer to $\sim 89^\circ/80^\circ$ and $\sim 92^\circ/80^\circ$ for the targeted DP = 100 and 200, respectively. These results indicated that more hydrophobic surface has been obtained as a consequence of linear *Pt*-BA brushes formation. Moreover, the contact angle hysteresis ($\theta_A - \theta_R$) being less than 20° also implies that the surface bearing *Pt*-BA brushes is quite homogeneous and smooth.

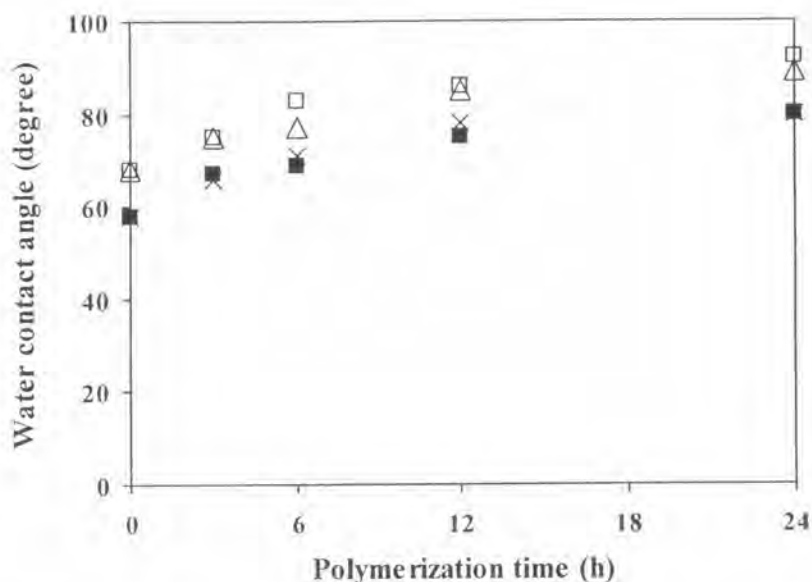
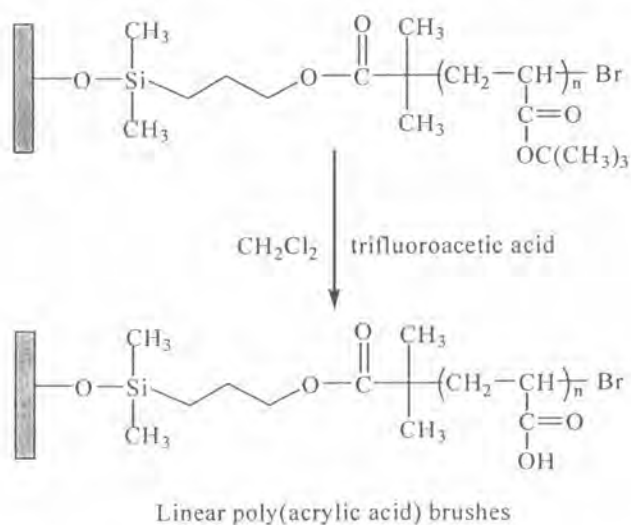


Figure 4.4 Water contact angle data of Pt-BA brushes versus polymerization time for targeted DP = 200 (θ_A (\square), θ_R (\blacksquare)) and 100 (θ_A (\triangle), θ_R (\times))

4.3 Preparation of Poly(acrylic acid) Brushes

PAA brushes can be prepared by hydrolysis of Pt-BA brushes using the optimal condition previously identified which is 2.5 M trifluoroacetic acid (TFA) in dichloromethane, room temperature and reaction time of 6 h.[85]



4.3.1 Confirmation of Poly(acrylic acid) Brushes Formation

Formation of PAA brushes on the silicon substrate was confirmed by FT-IR and contact angle analyses. Figure 4.5 shows FT-IR spectra of *Pt*-BA brushes ($\overline{M}_n = 20,760$ g/mole, targeted DP = 200) on silica particles before and after hydrolysis. After hydrolysis, the acid functionality is clearly visible. The broad peak ranging from 2800 to 3800 cm^{-1} was enhanced due to H-bonded carboxyl groups of PAA brushes. The carbonyl stretching of the ester group from *Pt*-BA brushes at 1727 cm^{-1} shifted slightly to 1716 cm^{-1} which belongs to the carbonyl stretching of the carboxyl group from PAA brushes. The contact angle of *Pt*-BA brushes has changed from 92°/80° to 33°/19° after hydrolysis indicating that the hydrophobic *Pt*-BA brushes were transformed to the hydrophilic PAA brushes.



Figure 4.5 FT-IR spectra of silica particles having *Pt*-BA brushes (a) and PAA brushes (b)

4.3.2 Determination of Carboxyl Group Density of Surface-tethered Poly(acrylic acid) Brushes

The density of carboxyl group (COOH) on PAA brushes was quantitatively determined by using toluidine blue O assay. The carboxyl groups of PAA brushes can form a complex with toluidine blue O. The absorbance of the solution containing the desorbed complex was measured at 633 nm. The COOH content was obtained from a calibration plot of the optical density versus dye concentration which is displayed in Appendix B. From Table 4.1, it was found that the calculated density of carboxyl group increased in proportion to the increase of the molecular weight of PAA brushes. These values correspond quite well with the theoretical values determined from the graft density of PAA brushes (See section 4.2.2 for detail). The fact that the toluidine blue O may also adsorb on the side of the substrate can be used to explain why the calculated carboxyl group densities are greater than the theoretical ones of which calculation is based on the ellipsometric and GPC data.

Table 4.1 Carboxyl group density (COOH) of surface-tethered PAA brushes

\overline{M}_n	Carboxyl group Density (mol/cm ²)	
	Theoretical Value	Calculated Value
13,983 (targeted DP = 100)	6.15×10^{-9}	7.10×10^{-9}
24,237 (targeted DP = 200)	11.30×10^{-9}	15.33×10^{-9}

4.4 Multilayer Assembly on Surface-tethered Poly(acrylic acid) Brushes

In this part of the studies, the surface-tethered PAA brushes were used as a substrate for multilayer assembly. Generated by “surface-initiated polymerization”, the graft density of the PAA brushes should be high enough to induce chain stretching allowing a thicker individual layer to be formed. If that is the case, the thicknesses of individual layer and multilayer should be varied as a function of PAA brushes thickness. In order to test the concept, two multilayer systems which are chitosan/poly(10,12-pentacosadiynoic acid) (PPCDA)) vesicles and chitosan/PAA were fabricated on the surface-tethered PAA brushes having two different molecular

weights and thicknesses. Chitosan (CHI) was chosen as cationic polyelectrolyte because it is natural polymer that possesses several interesting bioactivities that might be beneficial for the bio-related applications. The adsorption of CHI ($pK_a = 6.3-6.5$) was done at pH 4 so CHI was entirely protonated. The adsorption of both PAA and PPCDA having COOH groups ($pK_a = 4.50-4.75$) was conducted at pH 4 and 5.6, respectively. Thus, PAA was partly dissociated meaning that it exists in the form of carboxylate anion (COO^-) as well as carboxyl group (COOH) which is uncharged. Unlike PAA, PPCDA is completely dissociated at pH 5.6. Therefore, the assembly of the CHI/PAA multilayer should be driven by both hydrogen bonding and electrostatic attraction, whereas the assembly of CHI/PPCDA multilayer should mainly be driven by electrostatic attraction. The CHI/PPCDA vesicles multilayer formation was monitored by UV-Vis spectroscopy. The formation of the CHI/PAA multilayer was verified by FT-IR and contact angle analyses. The topography of the CHI/PAA multilayer film was also characterized by AFM.

4.4.1 The Influence of PAA Brushes Thickness on Multilayer Assembly

PPCDA vesicles were first selected as anionic species for multilayer assembly. The maximum absorption of UV-Vis light at the wavenumber of 640 nm of PPCDA vesicles allows the growth of CHI/PPCDA on glass-tethered PAA brushes to be conveniently monitored by UV-Vis spectroscopy. CHI as a cationic polyelectrolyte was deposited as the first layer followed by PPCDA. According to Figure 4.6, the absorbance at 640 nm increases linearly with the number of deposited layer indicating a stepwise growth of the multilayer between CHI and PPCDA. More importantly, it was observed that the absorbance of the multilayer grew from PAA brushes having $\overline{M}_n = 12,661$ was greater than that of the multilayer grew from PAA brushes having $\overline{M}_n = 9125$. These evidences implied that the amount of CHI as well as the PPCDA deposited depended upon the carboxyl group density of PAA brushes which can be varied as a function of the molecular weight of polymer brushes (See section 4.3.2). In addition, the quantity of the deposited layers can also be varied as a function of the deposition time. It can be seen from Figure 4.7 that the absorbance of

the glass-tethered PAA brushes adsorbed with a bilayer of CHI/PPDCA increases linearly as a function of deposition time. Obviously, the absorbance increment for the PAA brushes having higher \overline{M}_n was greater implying once again that the amount of CHI as well as the PPCDA depended upon the carboxyl group density of PAA brushes. This evidently suggests that the large quantity of the assembled film can be achieved without having to do a great number of deposition.

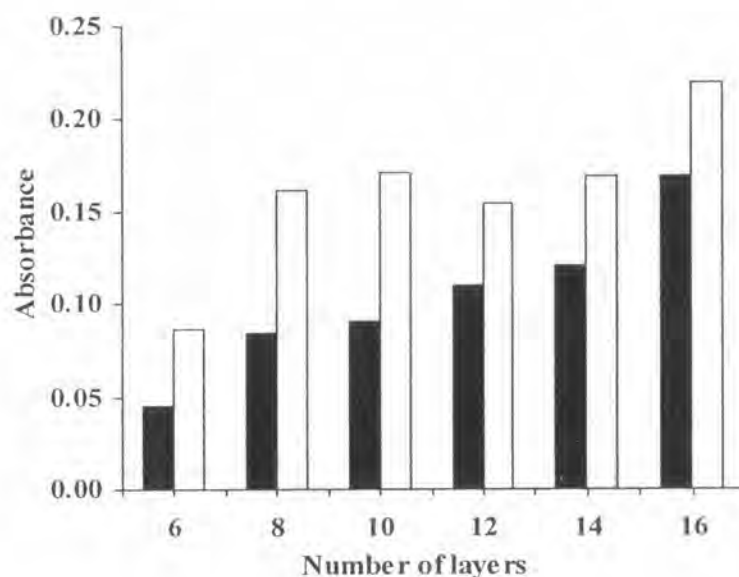


Figure 4.6 UV-Vis absorbance at 640 nm of CHI/ PPCDA vesicles multilayer (\overline{M}_n of CHI =100,000 g/mole) on glass-tethered PAA brushes having $\overline{M}_n = 9125$ (■) and 12661(□) as a function of number of layer

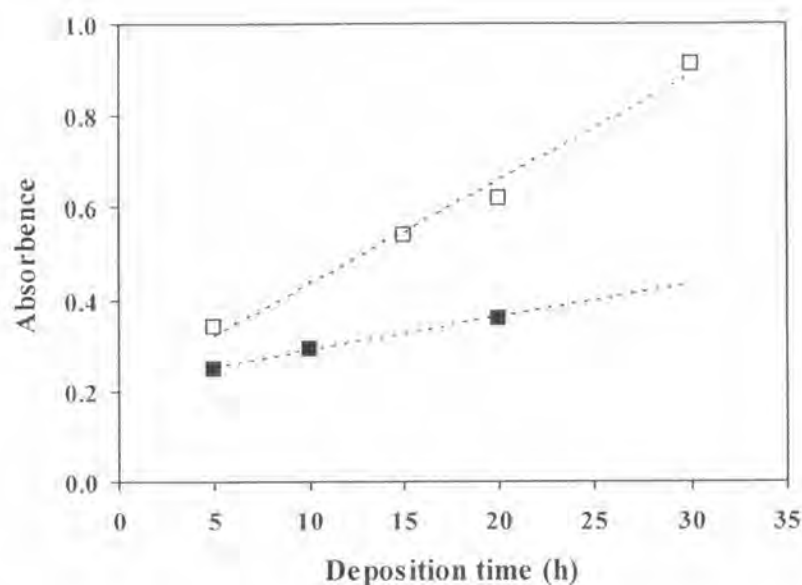


Figure 4.7 UV-Vis absorbance at 640 nm of a bilayer CHI/PPCDA vesicles (\bar{M}_n of CHI = 743,000 g/mole) on glass-tethered PAA brushes having $\bar{M}_n = 8343$ (■) and 11760(□) as a function of deposition time

To determine the effect of PAA brushes thickness on the thicknesses of individual layer and multilayer, the growth of CHI/PAA multilayer on the silicon-tethered PAA brushes were characterized by ellipsometry. Chitosan as a cationic polyelectrolyte was deposited as the first layer followed by PAA. The PAA brushes having two different \bar{M}_n and thickness were used for multilayer assembly. One has \bar{M}_n of 13,835 and the thickness of 6.7 nm. The other has \bar{M}_n of 24,797 and the thickness of 10.4 nm. The results shown in Figure 4.8 suggested that the thickness of the multilayer film proportionally increased as a function of the number of deposition on both substrates. Also, the thickness increment of each individual layer corresponded very well with the initial thickness of PAA brushes. One deposition step can elevate the thickness of as much as 5-10 nm. Thus, the thick multilayer film can easily be generated by using a thick PAA brushes as substrate. The thickness of the multilayer tended to level off after 8 deposition steps. It should be noted that the substrate with 9 layers appeared randomly opaque. It is thus assumed that there was some polymer aggregation taking place on the substrate causing the rough surface to

be formed. Thus, the uniform coating of the layer cannot be formed and the reliable thickness can no longer be measured by ellipsometry. This is the reason why we see the unchanged thickness beyond 8 layers. This speculation is later verified by AFM analysis. The results in this section implied that the graft density of PAA brushes was high enough to induce chain stretching and thereby allows a thicker individual layer to be formed.

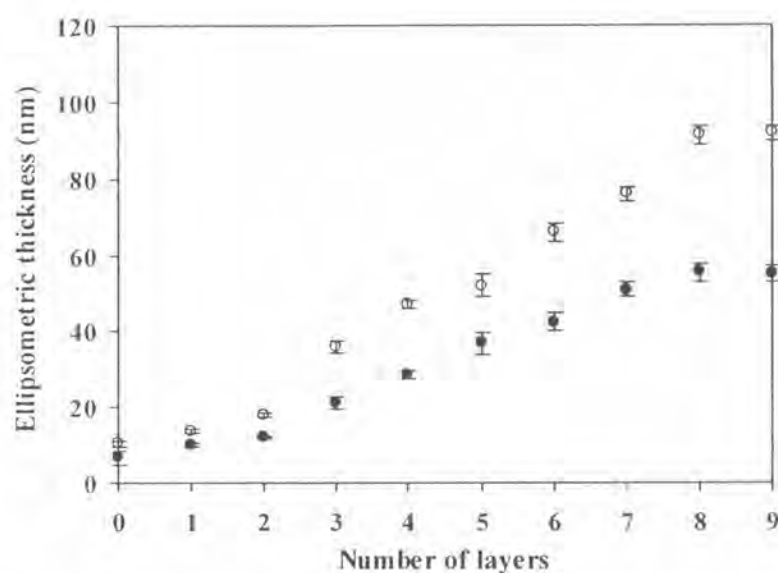


Figure 4.8 Ellipsometric thickness of CHI/PAA multilayer on silicon-tethered PAA brushes having $\overline{M}_n = 24,797$ (○) and 13,835 (●) as a function of number of layer

4.4.2 Confirmation of Chitosan/PAA Multilayer on Poly(acrylic acid) Brushes

FT-IR technique was used to characterize the functional groups of the CHI/PAA multilayer film on PAA brushes tethered to silica particles. In addition to the carbonyl stretching at 1716 cm^{-1} of PAA, the signal at 1548 cm^{-1} assigned to the N-H bending (amide II) appeared in the spectrum of CHI/PAA bilayer on PAA brushes (Figure 4.9 c) indicating the presence of CHI in the multilayer. Due to the masking of the signal from C-Si-O stretching of silica, the carbonyl stretching (amide I) of chitosan which should appear at 1650 cm^{-1} cannot be observed.

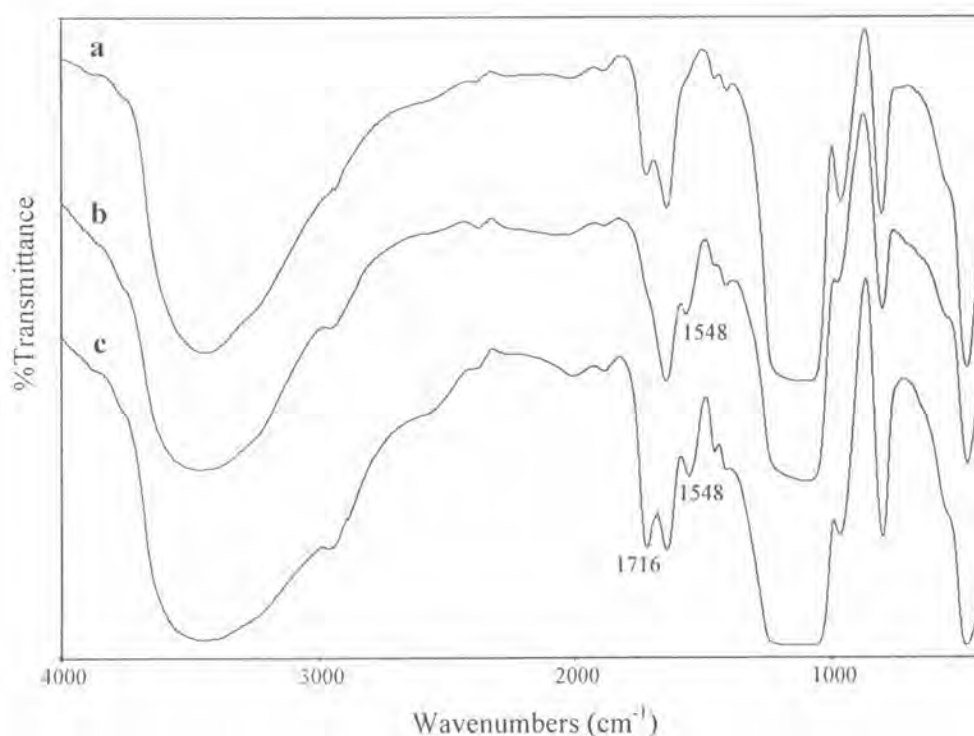


Figure 4.9 FT-IR spectra of silica particles having PAA brushes (a), 1 layer of CHI on PAA brushes (b) and CHI/PAA bilayer on PAA brushes (c)

If the concept of alternative adsorption is valid, the surface property of the multilayer film should alternately change. In other words, the multilayer film should be stratified. Water contact angle data shown in Figure 4.10 confirmed that the assembled film was stratified. The number appearing on the horizontal scale represented the number of deposition. If the number of layer is odd, CHI is the top layer and the charge of the outermost layer is positive. If the number of layer is even, PAA is the top layer and the charge of the outermost layer is negative. In this case, each individual layer are definitely thicker than the sampling depth of contact angle measurement (a few Å) so that the wettability of the multilayer film was strongly dependent on the last layer deposited and the influence of the underlying layers was not observed. The assembled film having the odd number of deposited layer (positively-charged surface) was clearly more hydrophobic than the one having the even number of deposited layer (negatively-charged surface). The results from contact

angle analysis also implied that other surface properties of the multilayer film such as surface topography, bioactivity should also be stratified.

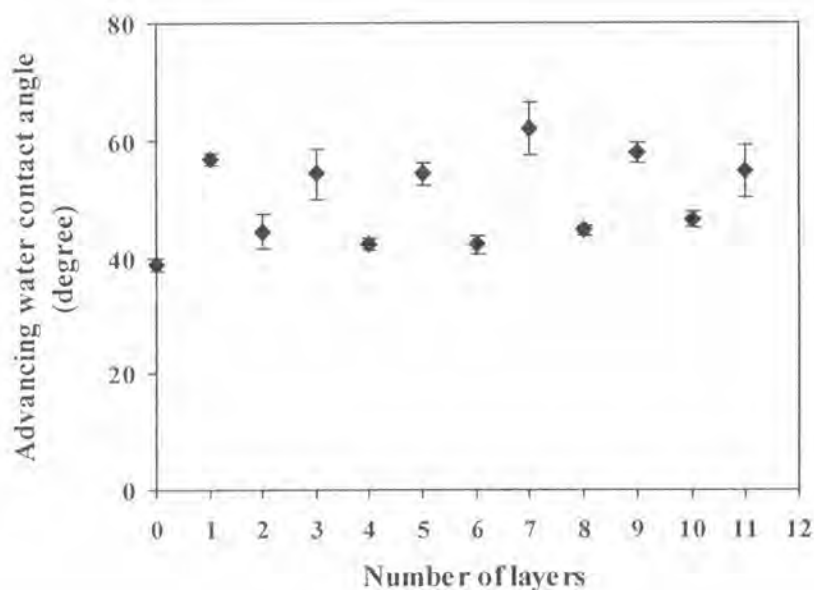


Figure 4.10 Water contact angle of CHI/PAA multilayer on surface-tethered PAA brushes

4.4.3 Surface Topography of CHI/PAA Multilayer on Poly(acrylic acid) Brushes

Atomic force microscopy (AFM) was used as a tool to determine the surface topography and roughness of the PAA brushes as well as the deposited multilayer. Similar to the cleaned silicon surface, AFM images of the *Pt*-BA brushes displayed in Figure 4.11 are almost featureless with relatively low surface roughness suggesting that the grafted *Pt*-BA brushes of both molecular weight are relatively smooth and uniform.

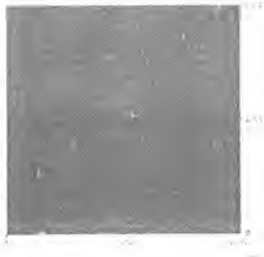
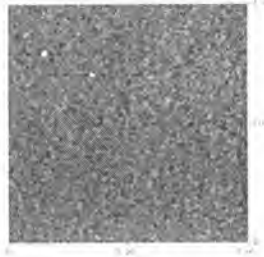
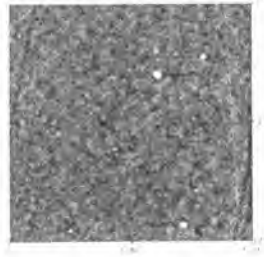
SiO₂	Pt-BA \bar{M}_n 13,784	Pt-BA \bar{M}_n 21,853
		
Roughness 0.089 nm	Roughness 0.243 nm	Roughness 0.290 nm

Figure 4.11 AFM images of surface-tethered Pt-BA brushes in comparison with the virgin silicon surface

AFM images shown in Figure 4.12 implied that the grafted PAA brushes of both molecular weights are relatively smooth and uniform similar to the grafted Pt-BA brushes. Also, the multilayer films having PAA as the top layer are obviously smoother than those having CHI as the top layer. The additional roughness introduced by the deposition of CHI progressively increases as a function of the number of layer. The size of the ripple-like feature of the multilayer having CHI as the top layer became correspondingly larger as the number of deposition increased. Interestingly, the roughness of the multilayer significantly decreased after it was covered by PAA suggesting that the roughness of the multilayer is also stratified. Having the same number of the deposited layer, the multilayer assembled on the PAA brushes with higher molecular weight are apparently rougher. This can be explained by the fact that the thicknesses of both the individual layer and overall multilayer are larger in the case of high molecular weight PAA brushes.

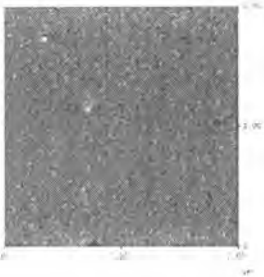
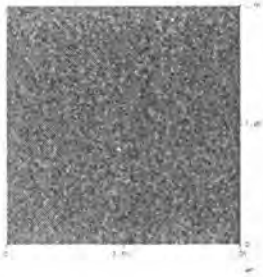
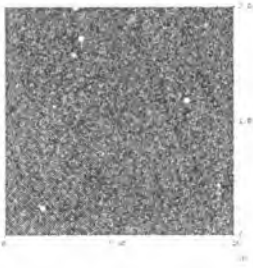
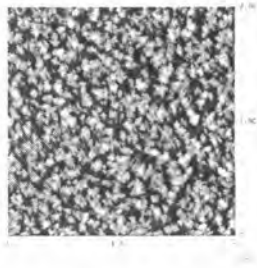
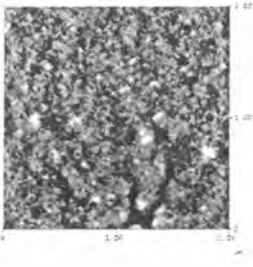
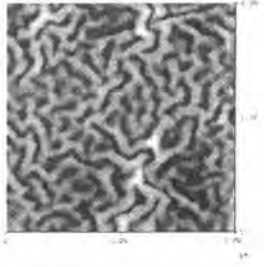
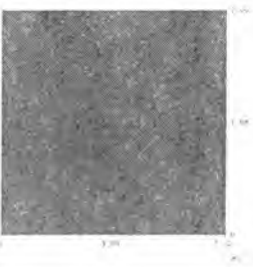
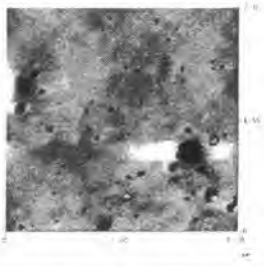
Sample	\bar{M}_n 13,784 g/mol	\bar{M}_n 21,853 g/mol
PAA brushes		
Roughness (nm)	0.193	0.238
CHI on PAA brushes (1 layer)		
Roughness (nm)	0.361	2.186
(CHI/PAA) ₂ CHI on PAA brushes (5 layers)		
Roughness (nm)	0.747	5.461
(Chitosan/PAA) ₃ on PAA brushes (6 layers)		
Roughness (nm)	0.018	0.575

Figure 4.12 AFM images of surface-tethered PAA brushes with CHI/PAA multilayer

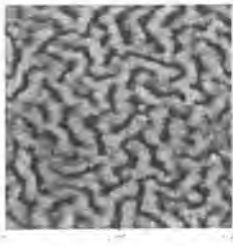
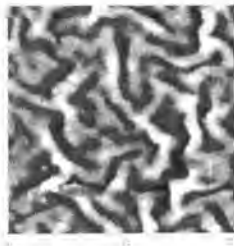
(CHI/PAA) ₃ CHI on PAA brushes (7 layers)		
Roughness (nm)	5.143	10.615

Figure 4.12 AFM images of surface-tethered PAA brushes with CHI/PAA multilayer (continue)

4.4.4 Stability of CHI/PAA Multilayer on Poly(acrylic acid) Brushes

The stability of the multilayer system is often of concern, especially in the environment that causes the displacement of the first adsorbed layer of polyelectrolyte and the subsequent desorption of the whole multilayer assembly i.e. changing the sign of the surface charge of the substrate or by addition of competing low molecular weight electrolytes. In this particular study, it is believed that the problem of the stability can be overcome since the PAA brushes are attached to the substrate by covalent bonds. To test the stability of the multilayer, the CHI/PAA multilayer on PAA brushes was subjected to soaking in buffer solutions having different pH for 24 h before being characterized by water contact angle and FT-IR analyses.

It can be demonstrated from Table 4.2 that the water contact angle of the multilayer became slightly higher after soaking in neutral and acidic buffer solution implying that the surface still holds the characteristic of CHI whose contact angle is higher than that of PAA (See Figure 4.10). In contrast, the water contact angle was a few degrees lower after soaking in basic buffer solution suggesting that the surface was somewhat more hydrophilic. This may be caused by the partial aggregation of CHI in the basic solution which made the underlying PAA more accessible to the contact angle measurement. According to the FT-IR spectra shown in Figure 4.13, it

is obvious that the common features and the relative peak intensity remained unchanged after the soaking independent of the pH of the buffer. Results from both techniques suggest that the multilayers are quite stable. Nonetheless, these results have not indicated that there was no polymer desorbed after the soaking. Such information require a more quantitative measure that is sensitive to the change of mass such as surface plasmon resonance (SPR) or quartz crystal microbalance (QCM).

Table 4.2 Advancing water contact angle of $(\text{CHI/PAA})_2\text{CHI}$ on PAA brushes before and after soaking in buffer solutions

Condition	Advancing water contact angle (degree)
Before soaking	43.6 ± 1.0
After soaking in buffer solution	
pH 3.5	44.8 ± 2.6
pH 7.4	46.8 ± 4.6
pH 10.0	39.9 ± 1.9

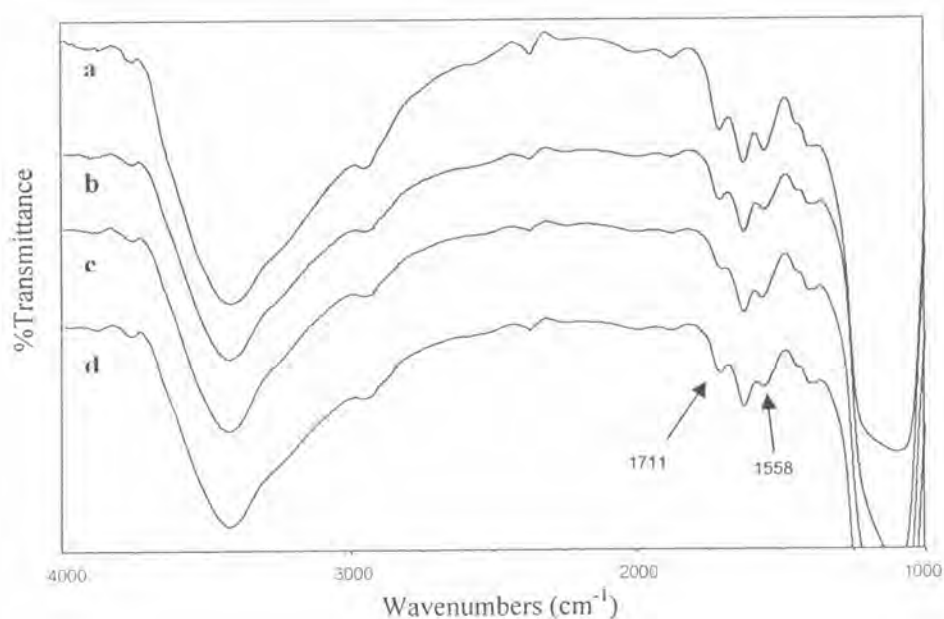


Figure 4.13 FT-IR spectra of silica particles having $(\text{CHI/PAA})_2\text{CHI}$ on PAA brushes before(a) and after soaking in buffer solution at pH 3.5 (b), pH 7.4 (c) and pH 10.0 (d)

4.5 Bioactivity Tests

It is important to determine whether the multilayer film deposited on the surface-tethered PAA brushes can be of practical uses. In particular, this study is interested in the bio-related applications of the multilayer film. Two tests are conducted: protein adsorption and antibacterial activity.

4.5.1 Protein Adsorption Test

Albumin protein, a carboxylic acid-rich protein, was selected for protein adsorption study. Its carboxylic acid group is converted to a negatively charged carboxylate ion at pH 7.4. The amount of adsorbed protein was determined by BCA assay. As shown in Figure 4.14, the adsorbed amount of albumin on the multilayer having an odd number of layers (CHI as the top layer) and a positive charge was higher than those having an even number of layers (PAA as the top layer) and a negative charge. Such a trend can be explained by the fact that the adsorption was promoted by electrostatic attraction between the positively-charged surface of the outermost layer and albumin. On the other hand, the adsorption of the negatively charged albumin was suppressed on the negatively charged surface having PAA as the top layer due to the electrostatic repulsion. The alternate trend is realized for both surface-tethered PAA regardless of the molecular weight. The roughness which increases as with the number of layer seems to influence the quantity of adsorbed protein. The rougher the surface, the greater the quantity of adsorbed protein.

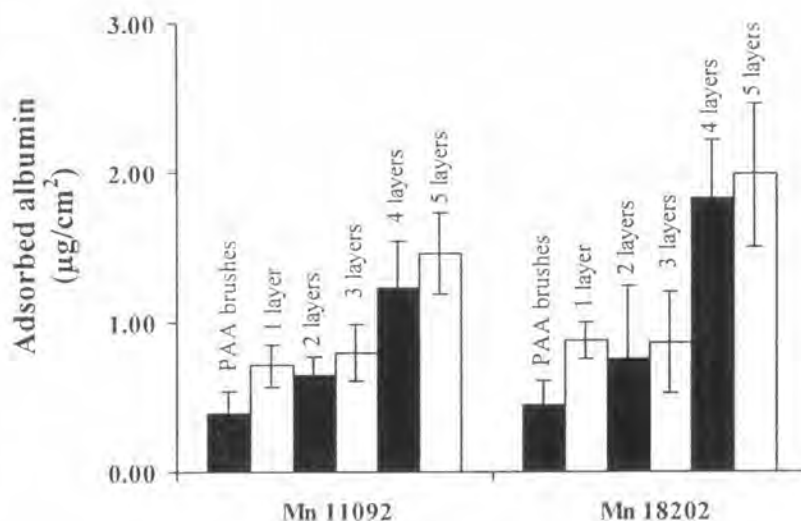


Figure 4.14 Amount of adsorbed albumin on CHI/PAA multilayer on PAA brushes. The number written above the bar graph is the number of layer

We also attempt to alter the bioactivity of the CHI/PAA multilayer by depositing other charged bioactive polyelectrolyte (Figure 4.15) as the top layer. The amount of adsorbed albumin on all multilayer films is outlined in Table 4.3. Apparently, the amount of adsorbed albumin decreased when the outermost layer was changed to HTACC and heparin indicating that the response to the protein was changed, especially in the case of heparin, a well-known protein-repelling polymer, whose charge characteristic is negative.



Figure 4.15 Chemical structures of HTACC and heparin

Table 4.3 Adsorbed albumin on CHI/PAA multilayer on PAA brushes.

Sample	Adsorbed albumin ($\mu\text{g}/\text{cm}^2$)
PAA brushes, $\overline{M}_n = 22391$	0.58 ± 0.13
(CHI-PAA) ₂	0.67 ± 0.19
(CHI-PAA) ₂ CHI	1.10 ± 0.30
(CHI-PAA) ₂ HTACC	0.67 ± 0.11
(CHI-PAA) ₂ CHI-heparin	0.39 ± 0.11

4.5.2 Antibacterial Test

We also attempted to test antibacterial activity of the multilayer films using the plate count method. In principle, the multilayer film having HTACC as the top layer should exhibit superior antibacterial activity to other systems. This is due to the presence of its positive quaternary moieties that can bind ionically with the bacteria membrane and thereby inhibits the growth of bacteria. Unfortunately, the number of viable bacteria after incubated with all multilayer films were so large that ones cannot differentiate the responses of all multilayer films from the control.